Double-walled carbon nanotube/zirconia composites: Preparation by spark plasma sintering, electrical conductivity and mechanical properties

Anne Kasperski, Alicia Weibel, Dalya Al-Kattan, Claude Estournès, Christophe Laurent, Alain Peigney

Double-walled carbon nanotube/zirconia composites: Preparation by spark plasma sintering, electrical conductivity and mechanical properties

A. Kasperski, A. Weibel*, D. Alkattan, C. Estournès, Ch. Laurent, A. Peigney

Université de Toulouse, Institut Carnot CIRIMAT, UPS CNRS, Université Paul-Sabatier, 31062 Toulouse cedex 9, France

Abstract

Double-walled carbon nanotube/yttria-stabilized zirconia composite powders with carbon contents up to 6.3 wt% are prepared by soft covalent functionalization of carbon nanotubes (CNTs) followed by mixing with a nanometric yttria-stabilized zirconia (YSZ) powder. Composites are densified by spark plasma sintering (SPS). The composites present an electrical conductivity (0.09–0.88 S cm^{-1}) which is among the highest values reported in the literature. Both the fracture strength (σ_f) and the single-edged notched beam fracture toughness (K_{Ic}) are measured for the first time on CNT/YSZ composites. The best mechanical properties ($\sigma_f = 694$ MPa; $K_{Ic} = 7$ MPa $m^{1/2}$), obtained for low carbon contents (up to 1.2 wt%), are among the highest reported up to now. However, the fracture toughness is lower than that of the YSZ ceramic ($K_{Ic} = 10.3$ MPa $m^{1/2}$) whose mechanical properties are outstanding, taking into account its very fine microstructure.

Keywords: Composites; Carbon nanotubes; Yttria stabilized zirconia (YSZ); Spark plasma sintering (SPS)

1. Introduction

Owing to the particular characteristics and exceptional properties of carbon nanotubes (CNTs), many works have been devoted for about two decades to the fabrication of novel composites including CNTs and the measurement of their properties in relationship to their composition and microstructure [1–5]. With a ceramic matrix, the main aims are to increase toughness, to improve the tribological properties or to control the electrical or thermal conductivities [3–5]. Although most studies have been related to CNT/alumina composites, some authors used yttria-stabilized zirconia (YSZ) as the matrix, in which they add either multi-walled CNTs (MWCNTs) [6–23] or single-wall CNTs (SWCNTs) [24–26]. Fracture toughness is often derived from indentation (ID) measurements, a method whose validity is contested by several authors, both for CNT/ceramic composites [27] and for ceramics [28]. However, despite the possible overestimation of the values, most CNT/YSZ composites show either a decrease [9,13] or a slight increase [6,10,18,19,22,23] of the fracture toughness compared to that of the corresponding YSZ. Only Mazheri et al. reported a marked increase (from 6.1 to 8.1 MPa $m^{1/2}$) both for the fracture toughness derived from the ID method [14] and the single-edged V-notched beam (SEVNB) method [15]. However, in stabilized zirconia, strength and toughness are disconnected, *i.e.* the higher toughness is obtained for low strength and conversely the higher strength is obtained for low toughness [29]. This is why, besides the measurement of fracture toughness, preferentially by a macroscopic method (SEVNB or SENB), that of the flexural strength is useful to get a proper evaluation of the performance of the material. Datye et al. measured the flexural strength of CNT/YSZ composites and showed an increase compared to YSZ (312 MPa *vs.* 257 MPa), but the reported values are low and they did not measure the fracture toughness [11]. Only Zhou et al. measured both and reported a slight strength increase but at a high value (990 MPa *vs.* 871 MPa) correlated with one of the highest reported ID fracture toughness (5.8 MPa $m^{1/2}$) [10]. Thus, further works are needed, including the measurements of both flexural strength and fracture toughness, to evaluate the possibility of using

*Corresponding author. Tel.: +33 561556175.
E-mail address: weibel@chimie.ups-tlse.fr (A. Weibel).

http://dx.doi.org/10.1016/j.ceramint.2015.08.034

CNT/zirconia composites instead of stabilized zirconia, particularly for biomedical applications [12,30]. Besides the expected gain in mechanical properties, many other points motivate such works. First, the preparation of stabilized zirconia with high fracture toughness remains difficult because it requires a tight control of the complex microstructure [31,32]. Second, the toughening effect by stress induced tetragonal-to-monoclinic phase transformation seems not to be effective with small grain sizes (<0.5 μm) [29]. Nevertheless, such a microstructure could be preferable in order to obtain a material less sensitive to ageing, a consequence of the tetragonal-to-monoclinic phase transformation in humid environment [13,30]. Third, some works have also shown that CNT/zirconia composites with 100 nm grains show a very low friction coefficient against alumina [20] or a low wear rate against Si_3N_4 [25].

An alternative way to the use of SWCNTs or MWCNTs to reinforce ceramics is that of double-walled CNTs (DWCNTs). Indeed, DWCNTs are a unique class of CNTs, with a formation mechanism similar to SWCNTs [5,33,34], and are possibly more interesting for composite applications because the outer wall could interact with the matrix, and also protect the inner wall from any damage [35]. For DWCNT/MgO composites, an unambiguous increase in both toughness and microhardness has been reported and the mechanisms of crack-bridging on an unprecedented scale, crack-deflection and DWCNT pullout have been evidenced [35]. With the alumina matrix, higher fracture strength and similar fracture toughness were also obtained for a similar submicronic grain size, and correlated with crack-bridging by CNTs on a large scale [36]. The aim of this work is to prepare DWCNT/yttria-stabilized ZrO_2 composites with zirconia grains about 100 nm in size, to characterize their microstructure and to measure their electrical conductivity and mechanical properties (microhardness, flexural strength and fracture toughness, the latter being measured by the single-edged notched beam (SENB) method).

2. Material and methods

2.1. Powder preparation

A commercial 3 mol% YSZ powder (TZ-3Y, Tosoh, Japan) was used for the study. The proportions of tetragonal and monoclinic ZrO_2 are 77 and 33 vol%, respectively. The average grain size is slightly lower than 100 nm [20]. DWCNTs were synthesized by the catalytic chemical vapor deposition (CCVD) route as reported earlier [37]. The $Mg_{0.99}(Co_{0.75}Mo_{0.25})_{0.010}O$ catalytic material was submitted to a CCVD treatment in H_2–CH_4 (18 mol% CH_4, heating and cooling rates 5 °C min^{-1}, maximum temperature 1000 °C, no dwell), producing a CNT/Co–Mo/MgO composite powder. This powder was soaked in a 37% HCl aqueous solution in order to dissolve MgO and most of the cobalt and molybdenum species, without damaging the CNTs [38]. The so-obtained suspension was filtered, washed with de-ionized water until neutrality, and kept wet (*i.e.* there was no drying step) in order to facilitate a further dispersion. The CNTs in the sample are mostly DWCNTs (80%), SWCNTs (15%) and CNTs with three walls (5%), with the outer diameter in the range 1–3 nm and the inner diameter in the range 0.5–2.5 nm [38]. The wet as-prepared DWCNTs were submitted to a soft functionalization using a mixture of nitric, sulphuric and chloridric acids at room temperature to achieve a satisfactory dispersion in deionized water [39]. Then, the mixture was neutralized with ammonia and filtered, taking care to keep the CNTs wet. The appropriate amount of acid-treated CNTs was dispersed in deionized water with a sonotrode for 15 min. The CNT suspension was poured into a suspension of zirconia in water (pH = 12) that was prepared previously (15 min sonication and 1 h mechanical stirring). The mixture was sonicated for 30 min. The vessel containing the DWCNT/YSZ suspension was immersed in liquid N_2 until freezing and was freeze-dried (Christ alpha 2–4 LD, Bioblock Scientific) at −84 °C for 48 h in a primary vacuum (residual pressure 12 Pa). The carbon content in the composite powders was measured by flash combustion with an accuracy of 2% (standard deviation calculated on ten measurements). The carbon content (C_w) in the DWCNT/YSZ composite powders is equal to 0.5, 1.2, 1.7, 4.5 and 6.3 wt% (Table 1).

2.2. Spark plasma sintering

The YSZ and DWCNT/YSZ powders were consolidated by spark plasma sintering (SPS, Dr Sinter 2080, SPS Syntex Inc., Japan). Into a 20 mm inner diameter graphite die were loaded, from bottom to top, a graphite punch, a sheet of graphitic paper, an alumina powder bed about 1.2 mm thick (in order to block the current and ensure a similar heating in specimens with a different electrical conductivity), a sheet of graphitic paper, the powder sample, then the same materials in reverse order. Graphitic paper was also placed along the circumference of the die for easy removal. SPS was performed in argon. A pulse pattern of 12 current pulses followed by 2 periods of zero current was used. A heating rate of 250 °C/min was used from room temperature to 600 °C, where a 3 min dwell was applied in order to stabilize the temperature reading. Then, the temperature was increased (heating rate 100 °C/min) from

Table 1
Carbon content in weight (C_w), I_D/I_G (%) ratio between the D and G bands of the Raman spectra for composite powders and sintered composites, SPS temperature and relative density. The I_D/I_G ratios have been calculated from three to six spectra depending on the sample; the minimum and maximum values (min–max) are also reported for the sintered composites.

Powders			Sintered ceramic and composites		
Label	C_w (wt%)	I_D/I_G	T (SPS) (°C)	I_D/I_G (min − max)	Relative density (%)
C0	0	–	1200	–	98
C0.5	0.5	0.16	1200	0.23 (0.09–0.72)	≈ 100
C1	1.2	0.03	1200	0.74 (0.45–1.46)	≈ 100
C2	1.7	0.17	1200	0.49 (0.37–0.61)	99
C4.5	4.5	0.13	1200	1.07 (0.69–1.31)	98
C6	6.3	0.12	1350	0.85 (0.33–1.20)	96

600 °C to its maximum value, either 1200 or 1350 °C according to the increasing carbon content (Table 1), where a 10 min dwell was applied. A uniaxial charge (corresponding to 100 MPa on the pellet) was gradually applied during the dwell at 600 °C and maintained during the remaining heating and the dwell at the maximum temperature. It was released within the last minute of the dwell. The cooling rate was equal to 60 °C/min. The sintered specimens were in form of pellets 8 and 20 mm in diameter and about 2 mm thick. The pellets were polished down to 1 μm using diamond slurries. The sintered specimens will be denoted C0, C0.5, C1, C2, C4.5 and C6 hereafter.

2.3. Characterization

The Raman spectra of the raw DWCNTs, composite powders and polished surfaces of sintered specimens were obtained with a Jobin-Yvon LabRAM HR 800 spectrometer (laser excitation at 632.82 nm). Three to six Raman spectra were averaged for each sample. The density of the pellets was measured by the Archimedes method after removal of the graphitic surface contamination layer by light polishing. The relative densities ($\rho \pm 1\%$) were calculated using 1.80 for DWCNTs and 6.05 g cm^{-3} for tetragonal zirconia. The fracture surfaces of the pellets were observed by field-emission-gun scanning electron microscopy (FESEM, JEOL JSM 6700F). The average zirconia grain size was determined from such images by the linear intercept method [40]. X-ray diffraction (XRD) patterns of the sintered specimens were recorded using a Bruker D4 Endeavor diffractrometer (Cu K_α radiation).

The electrical conductivity was measured on pellets 8 mm in diameter and about 2 mm thick using the capacitive method (metallization of the two faces of the pellet and measurement between the two electrodes). The measurements were performed at room temperature with direct currents using current densities lower than 160 mA/cm^2 (Keithley 2400). The indentation tests (300 g for 10 s in air at room temperature) were performed on the polished surface of the specimens by loading with a Vickers indenter (Shimadzu HMV 2000). The corresponding diagonals of the indentation pattern were measured using an optical microscope attached to the indenter. The calculated micro-hardness values are the average of 10 measurements. The transverse fracture strength (σ_f) was measured by the three-point bending method on parallelepipedic specimens about $1.8 \times 1.8 \times 18$ mm^3. Cross-head speed was fixed at 0.1 mm min^{-1}. The fracture toughness (K_{Ic}) was measured by the SENB method on similar specimens notched using a diamond wire 0.17 mm wide, using the calibration factor proposed by Brown and Srawley [41] for calculations. The values reported for σ_f and K_{Ic} (Table 2) are the average of measurements performed on six or seven specimens.

Table 2
Characteristics and properties of the specimens prepared by SPS. Carbon content in weight (C_w) and in volume (C_v), relative density, electrical conductivity (σ_e), Vickers microhardness (HV0.3), bending fracture strength (σ_f) and SENB fracture toughness (K_{Ic}). For the mechanical properties, standard deviations are reported.

Specimen	C_w (wt %)	C_v (vol %)	Relative density (%)	σ_e (S cm^{-1})	HV0.3 (GPa)	σ_f (MPa)	K_{Ic} (MPa m$^{1/2}$)
C0	0	0	98	$< 5.10^{-12}$	13.8 ± 0.6	692 ± 115	10.3 ± 1.3
C0.5	0.5	1.7	≈ 100	0.09	13.8 ± 0.6	694 ± 154	7.0 ± 1.3
C1	1.2	3.9	≈ 100	0.10	12.3 ± 0.8	526 ± 84	7.1 ± 0.9
C2	1.7	5.5	99	0.14	11.7 ± 0.1	507 ± 123	6.6 ± 3.4
C4.5	4.5	13.2	98	0.88	10.0 ± 2.8	333 ± 20	5.5 ± 3.1
C6	6.3	18.4	96	0.52	9.5 ± 0.7	223 ± 18	5.1 ± 0.7

3. Results and discussion

3.1. Microstructures

For all composite powders, the ratio between the intensities of the D band and the G band (I_D/I_G, Table 1) in the high-frequency range of the Raman spectra (not shown) is similar to that for the raw DWCNTs (0.03–0.17 *vs.* 0.11 ± 0.06). Thus, this shows that the covalent functionalization and the mixing process with zirconia did not damage the DWCNTs, contrary to what was reported for the preparation of DWCNT/Al_2O_3 composite powders using the same route ($I_D/I_G = 0.53$ *vs.* 0.13) [36]. This absence of damage to the DWCNTs probably results from the lower hardness of zirconia compared to alumina, thus limiting the consequences of friction and impact between the CNTs and ceramic grains.

Analysis of the XRD patterns and Raman spectra (Fig. 1a and b) reveals the presence of both tetragonal and monoclinic zirconia in the YSZ powder, but only the tetragonal form in the sintered sample. Thus, all the monoclinic zirconia grains present in the starting powder are transformed into tetragonal zirconia grains during sintering and retain this form at room temperature due to yttria-stabilization and relatively fast SPS cooling. Similar results were obtained for all composite specimens, showing that the DWCNTs do not affect the tetragonal phase retention. The relative densities (Table 1) are in the range 98–100% for C0 and C0.5–C4.5 . For C6, it is only 96% despite the higher sintering temperature (1350 °C *vs.* 1200 °C) applied because of the higher carbon content. As already evidenced by several authors [3–5], increasing the CNT content inhibits densification of the composite.

For all the sintered composites, an increase of the intensity of the D band is clearly observed on the Raman spectra (Fig. 2). The I_D/I_G ratios of the sintered composites are higher than that of the corresponding powders (Table 1). An increasing I_D/I_G value corresponds to a higher proportion of sp^3-like carbon, which is generally attributed to the presence of more structural defects in the CNTs. Moreover, for C1, C2 and C4.5, the broadening of the G band could be attributed to the D' band showing a high intensity (about one third that of the G band), a characteristic of very disordered carbons [42]. It thus appears that for the YSZ matrix composites, the SPS treatment induces damage to some DWCNTs, contrary to what is observed for the alumina matrix composites [36]. Ukai et al. reported the formation of some zirconium carbide after hot-isostatic-pressing of MWCNT/YSZ composites at 1450 °C [43]. No zirconium carbide was detected

on the present XRD patterns, probably because SPS was performed at lower temperatures and for shorter times. CNTs damage during SPS could more likely be in relation with the mixed ionic-electronic conductivity of the material at high temperatures [44]. Indeed, due to their high mobility, the O^{2-} anions could locally interact with the outer wall of the DWCNTs producing local damage. The wide dispersion of the I_D/I_G values shows that some DWCNTs are more prone to be damaged than others or that the phenomenon occurrence is unevenly distributed in the sample during SPS.

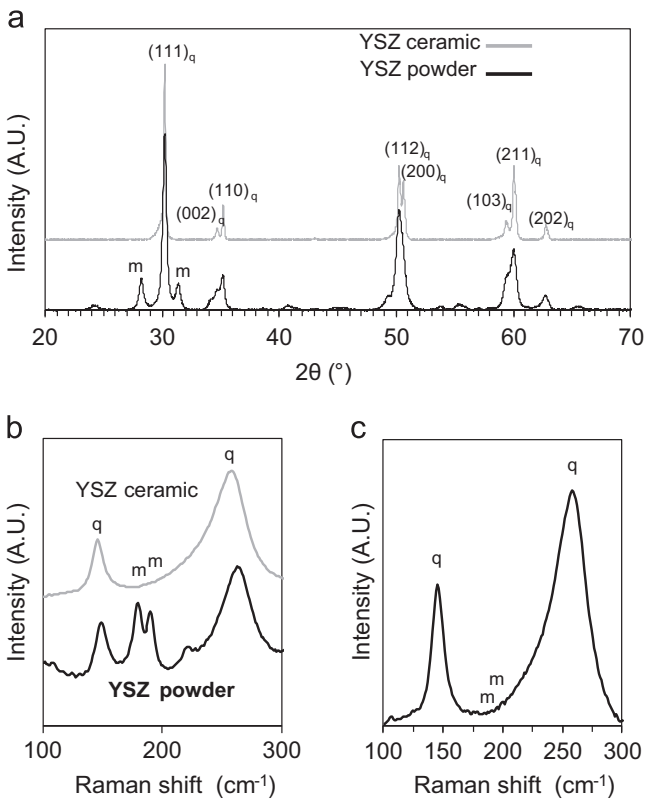

Fig. 1. XRD patterns (a) and Raman spectra (b) of the YSZ powder and sintered sample C0; Raman spectrum of the fracture surface of composite C2 (c).

FESEM observations of the fracture surfaces of the sintered specimens (Fig. 3) reveal an intergranular fracture mode for all samples, which facilitates the evaluation of grain sizes. The C0 sample (Fig. 3a) presents larger grains (195 nm) than composites samples sintered at the same temperature, C1 (Fig. 3b) and C2 (Fig. 3c), which show a grain size equal to 150 nm and 132 nm, respectively. This confirms that CNTs inhibit the grain growth of zirconia [9,13,15]. In most areas of the C6 sample (Fig. 3e and f), the grain size if slightly lower (~110 nm), despite a higher sintering temperature (1350 °C *vs.* 1200 °C) but some larger grains are also observed close to some residual pores (Fig. 3d). Long and flexible filaments corresponding to DWCNTs either isolated or in bundles appear to be well distributed at the grain boundaries of the zirconia matrix for C1 and C2 (Fig. 3b and c). For C6, agglomerates of long CNTs (Fig. 3d) and low-diameter bundles, either shorter or broken near the matrix surface, are present (Fig. 3e). At a higher magnification (Fig. 3f), some residues of CNTs are observed. These disordered carbon species mainly result from the shortening of the pristine CNTs, probably individual DWCNTs and low-diameter bundles which are less resistant to damage. FESEM observations of the C6 composite support the high I_D/I_G ratio (0.85), showing that an increase of the sintering temperature is detrimental to the CNTs structural

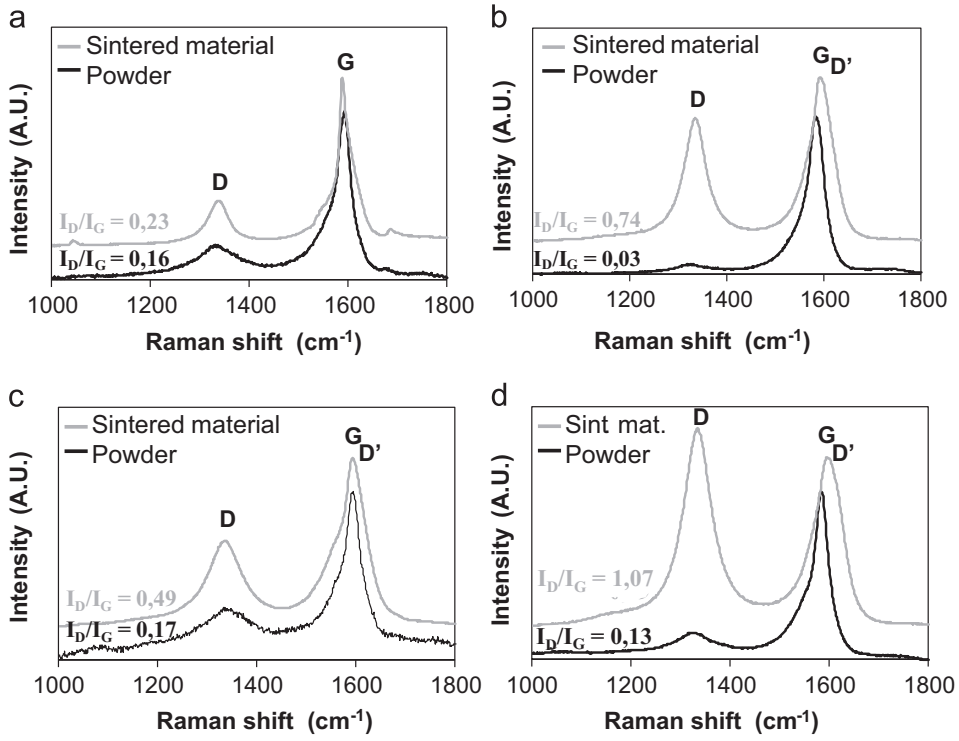

Fig. 2. Raman spectra of the composite powders and sintered samples: C0.5 (a); C1 (b); C2 (c); C4.5 (d).

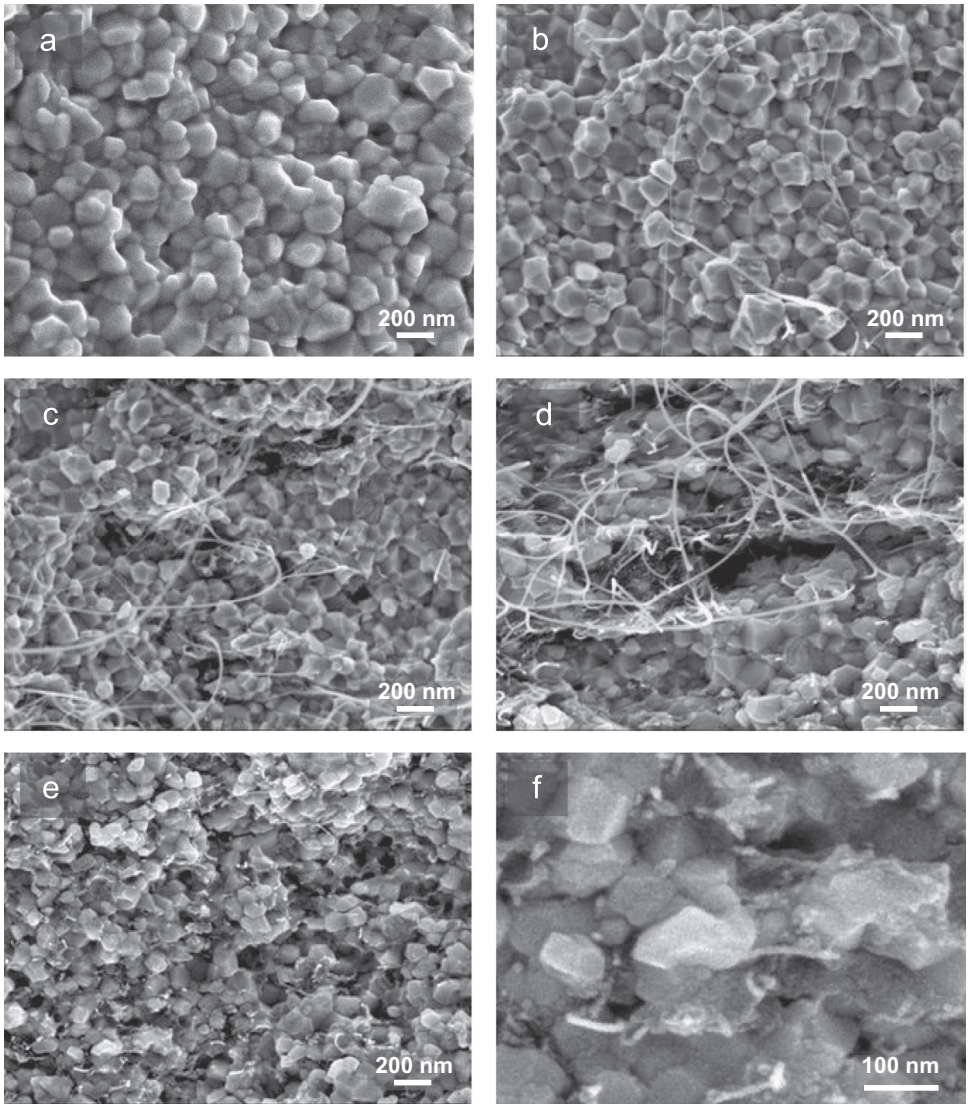

Fig. 3. SEM images of the fracture surfaces of sintered samples: C0 (a), C1 (b), C2 (c), C6 (d–f).

integrity. By contrast, despite the high I_D/I_G values for C1 (0.74) and C2 (0.49), CNTs residues were not observed by FESEM. At a lower sintering temperature (1200 °C), CNTs damage is mostly due to the creation of structural defects rather than to the formation of disordered carbon.

3.2. Electrical conductivity

All composites present an electrical conductivity of at least 0.09 S cm^{-1} (σ_e, Table 2), showing that the carbon content of these composites is higher than the percolation threshold. This is in agreement with the percolation thresholds measured both for SWCNT/YSZ composites (< 0.4 vol%) [25] and MWCNT/YSZ composites (< 0.75 vol%) [43]. The electrical conductivity for C0.5 is much higher than that reported by most authors for composites with the same carbon content but it is lower than that reported by Shin et al. (1 S cm^{-1}) [25] and Ukai et al. (0.58 S cm^{-1}) [43]. The difference in the measurement methods, volume capacitive measurement along the axis direction between the two faces of the pellets in the present work, surface measurement along the faces of the pellets for Shin et al. [25] and Ukai et al. [43] could explain this difference. Indeed, it is well known that in such materials there is a certain degree of alignment of the CNTs perpendicularly to the pressing axis, which results in an anisotropy of the electrical conductivity. The electrical conductivity increases with the carbon content, reaching a maximum (0.88 S cm^{-1}) for C4.5, and then decreases for C6. This decrease could be due to the lower homogeneity of the CNTs distribution in C6 and also to the higher damage sustained by the CNTs as evidenced by FESEM (Fig. 3d and f). Two groups reported values higher than 0.88 S cm^{-1} for similar carbon contents in SWCNT/YSZ composites [24,25], using the surface four probe measurement method, which could explain the difference. In fact, besides the differences in the measurement method and the direction of measurement, many parameters control the electrical conductivity of CNT/ceramic composites: the type of CNTs, degree of bundling, CNT dispersion homogeneity, CNT damage or lack thereof as well as the nature of the ceramic matrix. Moreover, for a given carbon

content, considering CNTs of equal length and similar bundling degree, SWCNTs are twice more numerous than DWCNTs [45], whereas the percentage of metallic CNTs is more than twice higher for a DWCNT sample than for a SWCNT sample [46]. Thus, it is not very easy to discriminate between all these parameters. Nevertheless, in the present work, the carbon contents and the high distribution homogeneity of the CNTs up to 4.5 wt% carbon (Fig. 3) are well correlated with the electrical conductivities of the composites, which are in the range of reported values.

3.3. Mechanical properties

The Vickers microhardness for C0 is equal to 13.8 GPa. It decreases smoothly with the increase in carbon content (Table 2), reaching 9.5 GPa for C6, the sample presenting the higher residual porosity (4%). The weak interfacial bonding between the CNTs and zirconia has been pointed out as responsible for the lower hardness of the composites in comparison with monolithic YSZ [26]. Nonetheless, these values are higher than those reported for MWCNT/YSZ composites [10,47] made using powders also prepared by a mixing route. The higher values obtained in the present study could reflect a better dispersion of CNTs in the matrix and/or the slightly lower matrix grain size. Contrary to all authors who reported mechanical properties of CNT/YSZ composites so far to the best of our knowledge, we measured both the fracture strength (σ_f) and fracture toughness (K_{Ic}), the latter using the SENB method to obtain more reliable values than those obtained when using the ID method. The fracture strength of C0 is high (about 690 MPa) and it is similar for C0.5. It decreases regularly from C1 to C6 upon the increase in the carbon content (Table 2). The SENB fracture toughness of C0 (10.3 MPa $m^{1/2}$ – Table 2) is the highest among those reported for such a ceramic with an average grain size below 200 nm [9,48–50], even when the measurements are made by the SEVNB method [15]. The fracture toughness of both C0.5 and C1 is still relatively high (about 7 MPa $m^{1/2}$). It decreases for higher carbon contents (C2–C6), with a distribution particularly wide for C2 and C4.5 (Table 2). This could reflect a lack of homogeneity in these two samples, although this was not detected by FESEM observations. However, with moderate DWCNT contents (up to 1.2 wt%, *i.e.* 3.9 vol% carbon), the fracture strength and fracture toughness reported together in the present work (Table 2) are almost the highest values among those reported, generally separately, for CNT/YSZ composites [9–12,17–19,23,25,26]. Only Zhou et al. [10] obtained a higher fracture strength (about 975 MPa), but with a lower fracture toughness (about 5.8 MPa $m^{1/2}$ by the ID method) for a 1 wt% MWCNT/YSZ composite, whereas Mazaheri et al. [15] reported a higher fracture toughness (about 10.9 MPa $m^{1/2}$ by the ID method but only 8 MPa $m^{1/2}$ by the SEVNB method) for a 5 wt% MWCNT/YSZ composite but without a report of the fracture strength. From XRD patterns recorded on the fracture surfaces, these authors evaluated that the amount of stress-induced tetragonal-to-monoclinic phase transformation decreased from about 36% for YSZ to about 23% for the 5 wt % MWCNT/YSZ composite. In the present work, using both XRD and Raman spectroscopy of the fracture surfaces (Fig. 1c), we did not detect the monoclinic phase for any of the samples. Thus, the reinforcement mechanism accounting for the high fracture toughness of the C0 sample remains to be elucidated. Maybe, more local characterizations are required to confirm the absence of any stress-induced tetragonal-to-monoclinic phase transformation near the cracks [18]. To investigate into more details the possible mechanisms of crack

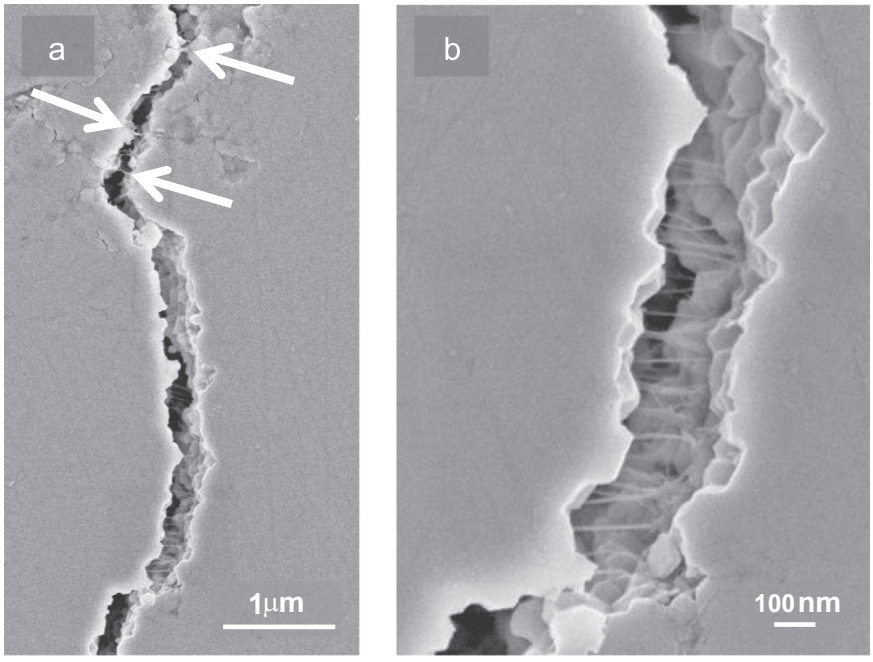

Fig. 4. SEM images of a crack made by Vickers indentation using a high load (2 kg) on C2: DWCNTs or DWCNT bundles bridging the crack in several areas (a); detail of the crack-bridging at a higher magnification (b).

deflection or crack bridging by the DWCNTs, Vickers patterns were performed on polished surfaces of the C2 composite using a high load (2 kg) in order to deliberately produce cracks, which were observed by FESEM (Fig. 4a and b). Crack-bridging by DWCNTs or bundles of DWCNTs is observed, either as isolated filaments (arrows in Fig. 4a) or, in some areas, by a large quantity of filaments (Fig. 4b). However, crack-bridging is not so homogeneous as was observed in a previous work for DWCNT/MgO composites for which the SENB toughness was doubled (6.7 MPa $m^{1/2}$ for the 2.3 wt% DWCNT/MgO composite against 3.4 MPa $m^{1/2}$ for MgO) [35]. And crack-bridging is not so extensive compared to what was observed for DWCNT/Al_2O_3 composites for which a fracture toughness similar to that of Al_2O_3 (5.4–5.6 MPa $m^{1/2}$) was reported for a low carbon content (2 wt%) [36]. Moreover, it is reasonable to think that the reinforcement of ceramic matrix composites by CNTs is all the more difficult when the fracture toughness of the corresponding ceramic is already high (10.3 MPa $m^{1/2}$ for ZrO_2 in the present work against only 3.4 MPa $m^{1/2}$ for MgO [36] and 5.4 MPa $m^{1/2}$ for Al_2O_3 [35]). Indeed, the high fracture toughness of a ceramic is generally the consequence of a particular reinforcement mechanism or of a particular microstructure for which the addition of CNTs could be unfavorable. In the present work, the observations let us think that the crack-bridging mechanism could contribute to maintain the fracture toughness at a high value in C0.5, C1 and in some of C2 SENB test samples, as reported by several authors for SWCNT/YSZ [25] and MWCNT/YSZ composites [12,15,47]. However, the damage to some DWCNTs induced by the SPS treatment, as revealed by Raman spectroscopy (Table 1), makes a homogeneous crack-bridging ineffective. Another consequence of DWCNT damage is the presence of disordered carbon at the grain boundaries. It leads to a loss of cohesion of the grain boundaries, which could decrease both the fracture strength and the fracture toughness. It remains to be tested if non-covalent functionalized DWCNTs [51] could be less prone to be damaged during the SPS treatment in the YSZ matrix than the covalent-functionalized DWCNTs used in the present work. The lower matrix grain size in the composites compared to the YSZ sample (135 nm *vs.* 195 nm) could also inhibit the reinforcement mechanisms operating in the YSZ sample.

4. Conclusion

DWCNTs have been used instead of SWCNTs or MWCNTs to prepare CNT/3 mol% yttria-stabilized zirconia (YSZ) composite powders with carbon contents up to 6.3 wt%. The quality of the DWCNTs is not altered during the powder preparation involving soft covalent functionalization of CNTs followed by dispersion and mixing with a nanometric YSZ powder by high energy sonication and freeze-drying. Composites were then almost fully densified by spark plasma sintering (SPS) at 1200 °C or 1350 °C depending on the carbon content. Contrary to what occurs with Al_2O_3 and MgO matrices, some DWCNTs are damaged during the SPS treatment, even at 1200 °C. For moderate carbon contents, the DWCNTs are well dispersed in the matrix, whose average grain size decreases from 195 nm for the YSZ ceramic to 110 nm for the 6 wt% DWCNT/YSZ composite. The electrical conductivities of the composites (between 0.09 and 0.88 S cm^{-1}) are among the highest reported for SWCNT and MWCNT/YSZ composites. Both the fracture strength (σ_f) and the SENB fracture toughness (K_{Ic}) were measured for the first time on CNT/YSZ composites. The best mechanical properties ($\sigma_f = 694$ MPa; $K_{Ic} = 7$ MPa $m^{1/2}$) are obtained for the lower carbon contents (up to 1.2 wt%) and are among the highest reported in the literature. However, the fracture toughness of the composites is lower than that of the YSZ ceramic ($K_{Ic} = 10.3$ MPa $m^{1/2}$) whose mechanical properties are outstanding, which is unusual for such a fine microstructure. Crack-bridging is observed in DWCNT/YSZ composites but it is not as homogeneous as that evidenced in DWCNT/MgO composites [35], probably because mainly of damaged DWCNTs. Non-covalent functionalized DWCNTs [51] could be less prone to be damaged during the SPS treatment in the YSZ matrix than the covalent-functionalized DWCNTs used in the present work. Thus, the use of low contents of DWCNTs remains promising for the reinforcement of CNT/YSZ composites.

Acknowledgements

SPS was performed at the Plateforme Nationale CNRS de Frittage-Flash (PNF^2, Toulouse). Electron microscopy was performed at the "Centre de microcaractérisation Raimond Castaing" – UMS 3623, Toulouse.

References

[1] S.R. Bakshi, D. Lahiri, A. Agarwal, Carbon nanotube reinforced metal matrix composites – a review, Int. Mater. Rev. 55 (2010) 41–64.
[2] J.N. Coleman, U. Khan, W.J. Blau, Y.K. Gun'ko, Small but strong: a review of the mechanical properties of carbon nanotube–polymer composites, Carbon 44 (2006) 1624–1652.
[3] J. Cho, A.R. Boccaccini, M.S.P. Shaffer, Ceramic matrix composites containing carbon nanotubes, J. Mater. Sci. 44 (2009) 1934–1951.
[4] E. Zapata-Solvas, D. Gomez-Garcia, A. Dominguez-Rodriguez, Towards physical properties tailoring of carbon nanotubes-reinforced ceramic matrix composites, J. Eur. Ceram. Soc. 32 (2012) 3001–3020.
[5] A. Peigney, A. Weibel, C. Laurent, Carbon nanotubes in ceramic–matrix nanocomposites, in: H.S. Nalwa (Ed.), American Scientific Publishers, Valencia, 2011, pp. 179–196.
[6] J. Sun, L. Gao, M. Iwasa, T. Nakayama, K. Niihara, Failure investigation of carbon nanotube/3Y-TZP nanocomposites, Ceram. Int. 31 (2005) 1131–1134.
[7] S.L. Shi, J. Liang, Electronic transport properties of multiwall carbon nanotubes/yttria-stabilized zirconia composites, J. Appl. Phys. 101 (2007) 023708 (1–5).
[8] S.L. Shi, J. Liang, The effect of multi-wall carbon nanotubes on electromagnetic interference shielding of ceramic composites, Nanotechnology 19 (2008) 255707 (1–5).
[9] A. Duszova, J. Dusza, K. Tomasek, G. Blugan, J. Kuebler, Microstructure and properties of carbon nanotube/zirconia composite, J. Eur. Ceram. Soc. 28 (2008) 1023–1027.
[10] J.P. Zhou, Q.M. Gong, K.Y. Yuan, J.J. Wu, Y.F. Chen, C.S. Li, J. Liang, The effects of multiwalled carbon nanotubes on the hot-pressed 3 mol% yttria stabilized zirconia ceramics, Mater. Sci. Eng. A – Struct. 520 (2009) 153–157.

[11] A. Datye, K.H. Wu, G. Gomes, V. Monroy, H.T. Lin, J. Vleugels, K. Vanmeensel, Synthesis, microstructure and mechanical properties of yttria stabilized zirconia (3YTZP) – multi-walled nanotube (MWNTs) nanocomposite by direct *in-situ* growth of MWNTs on Zirconia particles, Compos. Sci. Technol. 70 (2010) 2086–2092.

[12] N. Garmendia, I. Santacruz, R. Moreno, I. Obieta, Zirconia-MWCNT nanocomposites for biomedical applications obtained by colloidal processing, J. Mater. Sci. Mater. Med. 21 (2010) 1445–1451.

[13] N. Garmendia, S. Grandjean, J. Chevalier, L.A. Diaz, R. Torrecillas, I. Obieta, Zirconia-multiwall carbon nanotubes dense nano-composites with an unusual balance between crack and ageing resistance, J. Eur. Ceram. Soc. 31 (2011) 1009–1014.

[14] M. Mazaheri, D. Mari, R. Schaller, G. Bonnefont, G. Fantozzi, Processing of yttria stabilized zirconia reinforced with multi-walled carbon nanotubes with attractive mechanical properties, J. Eur. Ceram. Soc. 31 (2011) 2691–2698.

[15] M. Mazaheri, D. Mari, Z.R. Hesabi, R. Schaller, G. Fantozzi, Multi-walled carbon nanotube/nanostructured zirconia composites: outstanding mechanical properties in a wide range of temperature, Compos. Sci. Technol. 71 (2011) 939–945.

[16] M. Mazaheri, D. Mari, R. Schaller, High temperature mechanical spectroscopy of yttria stabilized zirconia reinforced with carbon nanotubes, Phys. Status Solidi A 207 (2010) 2456–2460.

[17] N. Garmendia, I. Santacruz, R. Moreno, I. Obieta, Influence of the addition of multiwall carbon nanotubes in the sintering of nanostructured yttria-stabilized tetragonal zirconia polycrystalline, Int. J. Appl. Ceram. Technol. 9 (2012) 193–198.

[18] R.K. Chintapalli, F.G. Marro, B. Milsom, M. Reece, M. Anglada, Processing and characterization of high-density zirconia-carbon nanotube composites, Mater. Sci. Eng. A – Struct. 549 (2012) 50–59.

[19] J. Yi, T. Wang, Z.P. Xie, W.J. Xue, Zirconia-based nanocomposite toughened by functionalized multi-wall carbon nanotubes, J. Alloy. Compd. 581 (2013) 452–458.

[20] A. Kasperski, A. Weibel, D. Alkattan, C. Estournes, V. Turq, C. Laurent, A. Peigney, Microhardness and friction coefficient of multi-walled carbon nanotube-yttria-stabilized ZrO_2 composites prepared by spark plasma sintering, Scr. Mater. 69 (2013) 338–341.

[21] L. Melk, J.J.R. Rovira, M.L. Antti, M. Anglada, Coefficient of friction and wear resistance of zirconia-MWCNTs composites, Ceram. Int. 41 (2015) 459–468.

[22] L. Melk, J.J.R. Roviraa, F. García-Marro, M.-L. Antti, B. Milsom, M. J. Reece, M. Anglada, Nanoindentation and fracture toughness of nanostructured zirconia/multi-walled carbon nanotube composites, Ceram. Int. 41 (2015) 2453–2461.

[23] W. Wu, Z. Xien, W.J. Xue, L. Cheng, Toughening effect of multiwall carbon nanotubes on 3Y-TZP zirconia ceramics at cryogenic temperatures, Ceram. Int. 41 (2015) 1303–1307.

[24] G.D. Zhan, J.D. Kuntz, A.K. Mukherjee, P.X. Zhu, K. Koumoto, Thermoelectric properties of carbon nanotube/ceramic nanocomposites, Scr. Mater. 54 (2006) 77–82.

[25] J.H. Shin, S.H. Hong, Microstructure and mechanical properties of single wall carbon nanotube reinforced yttria stabilized zircona ceramics, Mater. Sci. Eng. A – Struct. 556 (2012) 382–387.

[26] R. Poyato, A. Gallardo-Lopez, F. Gutierrez-Mora, A. Morales-Rodriguez, A. Munoz, A. Dominguez-Rodriguez, Effect of high SWNT content on the room temperature mechanical properties of fully dense 3YTZP/SWNT composites, J. Eur. Ceram. Soc. 34 (2014) 1571–1579.

[27] B.W. Sheldon, W.A. Curtin, Nanoceramic composites: tough to test, Nat. Mater. 3 (2004) 505–506.

[28] G.D. Quinn, R.C. Bradt, On the Vickers indentation fracture toughness test, J. Am. Ceram. Soc. 90 (2007) 673–680.

[29] J.R. Kelly, I. Denry, Stabilized zirconia as a structural ceramic: an overview, Dent. Mater. 24 (2008) 289–298.

[30] J. Chevalier, What future for zirconia as a biomaterial?, Biomaterials 27 (2006) 535–543

[31] R.H.J. Hannink, P.M. Kelly, B.C. Muddle, Transformation toughening in zirconia-containing ceramics, J. Am. Ceram. Soc. 83 (2000) 461–487.

[32] J. Chevalier, L. Gremillard, A.V. Virkar, D.R. Clarke, The tetragonal-monoclinic transformation in zirconia: lessons learned and future trends, J. Am. Ceram. Soc. 92 (2009) 1901–1920.

[33] J.H. Hafner, M.J. Bronikowski, B.R. Azamian, P. Nikolaev, A.G. Rinzler, D.T. Colbert, K.A. Smith, R.E. Smalley, Catalytic growth of single-wall carbon nanotubes from metal particles, Chem. Phys. Lett. 296 (1998) 195–202.

[34] A. Kasperski, A. Weibel, L. Datas, E. De Grave, A. Peigney, C. Laurent, Large-diameter single-wall carbon nanotubes formed alongside small-diameter double-walled carbon nanotubes, J. Phys. Chem. C 119 (2015) 1524–1535.

[35] A. Peigney, F.L. Garcia, C. Estournes, A. Weibel, C. Laurent, Toughening and hardening in double-walled carbon nanotube/nanostructured magnesia composites, Carbon 48 (2010) 1952–1960.

[36] A. Kasperski, A. Weibel, C. Estournes, C. Laurent, A. Peigney, Preparation-microstructure-property relationships in double-walled carbon nanotubes/alumina composites, Carbon 53 (2013) 62–72.

[37] E. Flahaut, R. Bacsa, A. Peigney, C. Laurent, Gram-scale CCVD synthesis of double-walled carbon nanotubes, Chem. Commun. 12 (2003) 1442–1443.

[38] E. Flahaut, A. Peigney, C. Laurent, A. Rousset, Synthesis of single-walled carbon nanotube Co–MgO composite powders and extraction of the nanotubes, J. Mater. Chem. 10 (2000) 249–252.

[39] M.J. de Andrade, M.D. Lima, V. Skakalova, C.P. Bergmann, S. Roth, Electrical properties of transparent carbon nanotube networks prepared through different techniques, Phys. Status Solidi – Rapid Res. Lett. 1 (2007) 178–180.

[40] M.I. Mendelsohn, Average grain size in polycrystaline ceramics, J. Am. Ceram. Soc. 52 (1969) 443.

[41] W.F. Brown, J.E. Srawley, Plane strain crack toughness testing of high strength metallic materials, ASTM Special Technical Publication, ASTM, Philadelphia, PA, 1966.

[42] R. Vidano, D.B. Fischbach, New lines in Raman-spectra of carbons and graphite, J. Am. Ceram. Soc. 61 (1978) 13–17.

[43] T. Ukai, T. Sekino, A. Hirvonen, N. Tanaka, T. Kusunose, T. Nakayama, K. Niihara, Preparation and electrical properties of carbon nanotubes dispersed zirconia nanocomposites, in: T.S. Ohji, T. Niihara, K. (Eds.), Trans Tech Publications, Pfaffikon, 2006, pp. 661–664.

[44] F.C. Fonseca, R. Muccillo, D.Z. de Florio, L.O. Ladeira, A.S. Ferlauto, L. O. Ladeira, A.S. Ferlauto, Mixed ionic-electronic conductivity in yttria-stabilized zirconia/carbon nanotube composites, Appl. Phys. Lett. 91 (2007) 243107 (1–3).

[45] C. Laurent, E. Flahaut, A. Peigney, The weight and density of carbon nanotubes *versus* the number of walls and diameter, Carbon 48 (2010) 2994–2996.

[46] F. Seichepine, S. Salomon, M. Collet, S. Guillon, L. Nicu, G. Larrieu, E. Flahaut, C. Vieu, A combination of capillary and dielectrophoresis-driven assembly methods for wafer scale integration of carbon-nanotube-based nanocarpets, Nanotechnology 23 (2012) 095303.

[47] N. Garmendia, I. Santacruz, R. Morenob, I. Obieta, Slip casting of nanozirconia/MWCNT composites using a heterocoagulation process, J. Eur. Ceram. Soc. 29 (2009) 1939–1945.

[48] M. Muroi, G. Trotter, P.G. McCormick, M. Kawahara, M. Tokita, Preparation of nano-grained zirconia ceramics by low-temperature, low-pressure spark plasma sintering, J. Mater. Sci. 43 (2008) 6376–6384.

[49] Y. Hou, C. Li, L. Wang, Y. Ding, Investigation into the mechanical properties of nanometric zirconia dentals ceramics, in: R. Chen (Ed.), Proceedings of International Conference on Mechatronics And Intelligent Materials, Trans Tech Publications, Pfaffikon, 2011, pp. 31–35.

[50] O. Bezdorozhev, H. Borodianska, Y. Sakka, O. Vasylkiv, Tough yttria-stabilized zirconia ceramic by low-temperature spark plasma sintering of long-term stored nanopowders, J. Nanosci. Nanotechnol. 11 (2011) 7901–7909.

[51] A. Kasperski, A. Weibel, C. Estournes, C. Laurent, A. Peigney, Multi-walled carbon nanotube-Al_2O_3 composites: covalent or non-covalent functionalization for mechanical reinforcement, Scr. Mater. 75 (2014) 46–49.